frontiers | Frontiers in Chemistry

TYPE Original Research
PUBLISHED 03 February 2023
DOI 10.3389/fchem.2023.1034473

Check for updates

OPEN ACCESS

EDITED BY
Hani Nasser Abdelhamid,
Assiut University, Egypt

REVIEWED BY
Walid Sharmoukh,
National Research Centre, Egypt
Mervat Ibrahim,
Soochow University, China

*CORRESPONDENCE
Asif Ur Rehman,
asyf.rehman@gmail.com
Abid Ullah,
abidmech95@gmail.com
Tingting Liu,
liutingting@njust.edu.cn

SPECIALTY SECTION
This article was submitted to Green and Sustainable Chemistry, a section of the journal Frontiers in Chemistry

RECEIVED 01 September 2022
ACCEPTED 20 January 2023
PUBLISHED 03 February 2023

CITATION
Ur Rehman A, Ullah A, Liu T, Ur Rehman R and Salamci MU (2023), Additive manufacturing of Al_2O_3 ceramics with MgO/SiC contents by laser powder bed fusion process.
Front. Chem. 11:1034473.
doi: 10.3389/fchem.2023.1034473

COPYRIGHT
© 2023 Ur Rehman, Ullah, Liu, Ur Rehman and Salamci. This is an open-access article distributed under the terms of the Creative Commons Attribution License (CC BY). The use, distribution or reproduction in other forums is permitted, provided the original author(s) and the copyright owner(s) are credited and that the original publication in this journal is cited, in accordance with accepted academic practice. No use, distribution or reproduction is permitted which does not comply with these terms.

Additive manufacturing of Al_2O_3 ceramics with MgO/SiC contents by laser powder bed fusion process

Asif Ur Rehman[1,2,3]*, Abid Ullah[2,3,4]*, Tingting Liu[5]*, Rashid Ur Rehman[6] and Metin U. Salamci[2,3,7]

[1]ERMAKSAN, Bursa, Türkiye, [2]Department of Mechanical Engineering, Faculty of Engineering, Gazi University, Ankara, Türkiye, [3]Additive Manufacturing Technologies Research and Application Center-EKTAM, Gazi University, Ankara, Türkiye, [4]CAS Key Laboratory of Mechanical Behavior and Design of Materials, Department of Modern Mechanics, University of Science and Technology of China, Hefei, Anhui, China, [5]School of Mechanical Engineering, Nanjing University of Science and Technology, Nanjing, Jiangsu, China, [6]Incheon National University, Incheon, South Korea, [7]Advanced Manufacturing Technologies Center of Excellence-URTEMM, Ankara, Türkiye

Laser powder bed fusion is a laser-based additive manufacturing technique that uses a high-energy laser beam to interact directly with powder feedstock. LPBF of oxide ceramics is highly desirable for aerospace, biomedical and high-tech industries. However, the LPBF of ceramics remains a challenging area to address. In this work, a new slurry-based approach for LPBF of ceramic was studied, which has some significant advantages compared to indirect selective laser sintering of ceramic powders. LPBF of Al_2O_3 was fabricated at different MgO loads up to 80 wt%. Several specimens on different laser powers (70 W–120 W) were printed. The addition of magnesia influenced the microstructure of the alumina ceramic significantly. The findings show that when the laser power is high and the magnesia load is low, the surface quality of the printing parts improves. It is feasible to produce slurry ceramic parts without binders through LPBF. Furthermore, the effects of SiC and MgO loads on the microstructure and surface morphology of alumina are compared and analysed.

KEYWORDS

additive manufacturing, sintering, defects, ceramic, oxidation, laser processing

Introduction

Complex shape ceramic components are manufactured utilizing a variety of traditional processes, such as hot isostatic pressing, extrusion, injection modelling, casting, and so on (Kingery, 1958). All conventional methods require more time and expensive tools such as drilling, milling gear shapers, and grinding machines to manufacture a part (Prakash et al., 2021). Additive Manufacturing (AM), widely known as 3D Printing, refers to a series of manufacturing methods in which parts and articles (3D objects) are made by layering materials (Redwood, 2018; Ullah et al., 2020; Ahmed et al., 2021). The fundamental working principles for additive manufacturing techniques are to add materials in a layer-by-layer fashion, however, the method with which materials are deposited and joined to make 3D objects differs between processes (Ansari et al., 2021; Kumar and Sharma, 2021; Mahmood et al., 2022). Laser powder bed fusion (LPBF), also widely recognized as selective laser melting (SLM), is a common laser-based AM technology that operates on the layer-by-layer manufacturing principle. LPBF can be used to fabricate three-dimensional ceramic parts directly, without using a sacrificial binder (Deckers et al., 2014a; Zhang et al., 2018; Aktrk et al., 2021; Rehman et al., 2021; Korkmaz et al., 2022a). This is the only direct method for printing pure ceramics. Other processes, including binder jetting, robocasting, and fused deposition of ceramics, are utilized to print ceramics,

although these methods require binders or certain fibers to be added. Similarly, selective laser sintering (SLS) technology requires adding a binder to the raw material powder, while SLM can fabricate parts without utilizing any binders (Kruth et al., 2005). Direct printing of ceramics without using an external binder or additives is the key advantage of the SLM process. LPBF is preferred over other AM processes for a variety of reasons, including the feature that it is a "single-step" process that does not require any special post-processing processes. Throughout one-step powder bed fusion by complete melting, the laser beam causes the deposited material powder to heat and fully melt (Deckers et al., 2014b; Dezfoli et al., 2021a; Waqar et al., 2021a; Dezfoli et al., 2021b; Waqar et al., 2022). However, the whole system produces a very high-temperature gradient and residual stresses due to the rapid heating and cooling of printed layers (Sing et al., 2017; Waqar et al., 2021b; Korkmaz et al., 2022b; Khan et al., 2022). This is believed to be a severe issue for printing ceramics and composites due to their low thermal shock resistance (Zhang et al., 2022). Researchers have studied numerous individual aspects that affect the LPBF method, such as pre-heating, the surrounding temperature, scan speed, hatch distance, beam power, intervals duration, scanning strategy (orthogonal, islands, zigzag pattern, and many others), the effects of the non-steady-state melt regimes in the scanning tracks, the role of pores on crack initiation, laser pre-heating of ceramic material, powder particle density, and so on (Yamakov et al., 2002; Wilkes et al., 2013; Schwentenwein and Homa, 2015; Wang et al., 2017; Liu et al., 2020; Waqar et al., 2021b; Gokcekaya et al., 2021; Abdelmoula et al., 2022; Sun et al., 2022; Wang et al., 2022). Directly manufacturing highly dense ceramics with LPBF might result in fractures and other manufacturing flaws (Yamakov et al., 2002; WIPO, 2018). Abnormal grains form during the direct manufacturing of ceramics, resulting in severe component defects such as fractures and poor mechanical properties (Yamakov et al., 2002; Rahaman, 2017). In order to achieve a homogeneous and higher density, it is necessary to control abnormal grain growth. Therefore, further investigation of component defects and overcoming these defects is required. The addition of other materials to ceramic is one of the key approaches which can enhance manufacturability (Harun et al., 2012). The use of additives offers a very significant approach for fabricating ceramic with high density and controlled grain size structure (Rice, 2017). As MgO has a greater melting temperature (2,800°C–3,000 °C) than Al_2O_3, which has a melting temperature of 2,300 °C, it can increase manufacturability through crack deflection and pinning effect (Wu et al., 2001). Previous findings support that MgO enabled the ceramic structure become denser and enhancing physical and mechanical properties (Sathiyakumar and Gnanam, 2003; Harun et al., 2012).

Laser powder bed fusion of Alumina with Magnesia has tremendous opportunities and challenges as well. Composite materials consisting of a strengthening phase started developing very early. The reinforcements can be as particulate or as fibers. While these composite materials show great promise of improved strength and stiffness in the fabrication of parts. A preferable combination of several important properties such as high melting point, good thermal shock resistance, high resistance to chemical attack, high electrical resistivity, low thermal expansion coefficient, and potentially high mechanical strength at different temperatures, have made magnesium aluminate ($MgAl_2O_4$) very attractive for engineering applications (Stewart and Bradt, 1980; Baudin et al., 1995; Ganesh, 2013; Peng et al., 2021). Magnesium aluminate has drawn attention from the industries in the field of metallurgical, radio technical and electrochemical, chemical industries because of its excellent properties and environmental advantages (Peng et al., 2021). These functional properties make magnesium aluminate a good quality and superior variety of refractory material. It is also a commercially important ceramic reinforcement for metal matrix composites (MMC) fabrication because of its tailorable and functional properties. The Manufacturing of magnesium aluminate and the method for making refractories were available in the form of patents since 1905 (Sarkar, 2010). However, its higher cost of fabrication and production *via* traditional manufacturing techniques has limited its commercial acceptance.

LPBF offers the possibility of rapid manufacturing of ceramic composites which can have great promising applications unconstrained of their shapes. The studies were carried out using the eutectics phase diagram of alumina and magnesia as a reference (Callister, 2000). Magnesia is soluble in alumina at various temperatures and compositions. The solubility of a substance changes as its composition changes. Since solubility is affected by temperature, the same composition might have various levels of solubility at different temperatures. The purpose of this work is to examine how density and porosity changed as material proportions changed, in order to make dense pieces and reduced surface defects. The influence of LPBF process parameters and MgO content on the microstructure, density, and surface quality of Alumina parts are investigated in detail. The phase shift that occurs during the melting and sintering of the powder is also analyzed. In addition, the effects of SiC and MgO additions on the alumina microstructure and surface are analyzed and compared. This study will also investigate the optimal process parameters for Al_2O_3/MgO composite materials, in order to reduce major part defects and improve the overall ceramics manufacturing process using the LPBF technology.

Experimental

Materials and methods

In this work MgO powders (Shanghai Chaowei Nanotechnology Co., Ltd.) of average particle size 1 μm and Al_2O_3 powder (produced by ALMATIS) of average particle size 0.4 μm with 99.9% purity were used for the experiments. The powders have irregular sheet structure, as shown in Figure 1. Several compositions with differing quantities of alumina and magnesia were sintered and melted. The experiments were performed with changing laser power while laser scanning speed and other process parameters such as hatch distance, layers thickness, and layers numbers were kept constant. Table 1 shows the experimental process parameters.

Layer deposition method

Layer deposition of pure ceramics is difficult to maintain due to the inherent characteristics of ceramic powder. In this work, a two-step deposition method was used during the layer deposition process. Firstly, the powder was mixed with water as per the suitable material composition, resulting in a slurry that was deposited on the ceramic substrate fixed inside the layer moveable platform. The experimental platform has a powder leveling system, which is equipped with a rubber scraper. The scraper was used to spread and level the powder

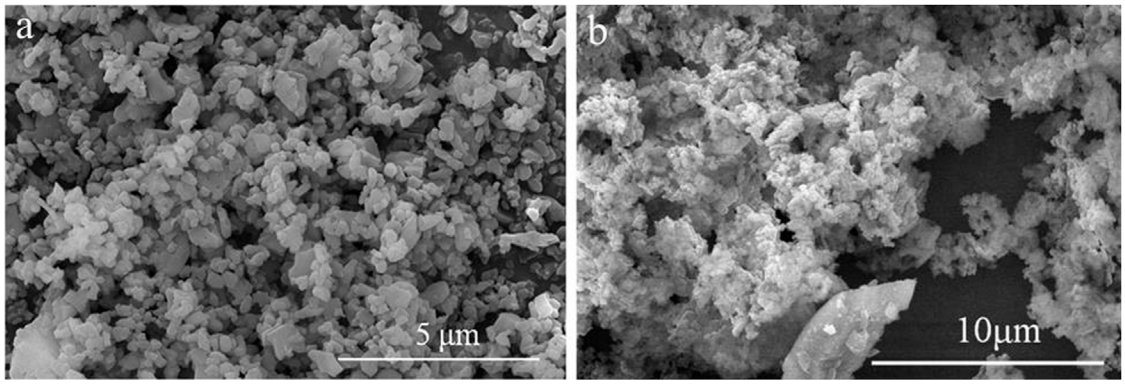


FIGURE 1
(A) Al_2O_3 powder **(B)** MgO powder (Zheng et al., 2019)

TABLE 1 Experimental process parameters.

Material (wt%)	Laser power W)	Scanning speed (mm/s)	Layer thickness (μm)	Hatch spacing (μm)	Scanning strategy
Al_2O_3: MgO = 20:80	70, 90, 110	200	50	50	Zigzag
Al_2O_3: MgO = 30:70					
Al_2O_3: MgO = 60:40					
Al_2O_3: MgO = 90:10					

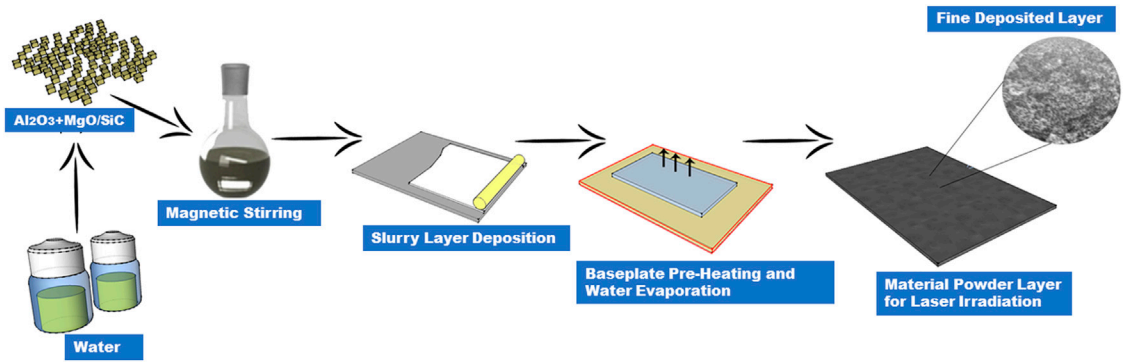


FIGURE 2
Layer deposition method.

slurry in layers. The platform thickness of moveable systems can be extended from as smaller as 10 μm. The thickness of each layer was maintained as 50 μm. After the proper layer deposition, the water was fully evaporated by heating the base plate to 110 °C. The deposited layers appeared uniform when the water was evaporated, with no obvious deformities or differences between the top and bottom of the dried layers. The power layer was melted by directing the laser beam. The entire layer deposition process was repeated until the final part was produced with the required number of layers. Figure 2 illustrates the whole layer deposition process. The main objective of the slurry in this work was to make a homogeneous paste and appropriately deposit the layers according to the experimental requirements. The slurry approach was also used in the previous research for the manufacturing of alumina ceramic parts by digital light processing (DLP) based AM technique which plays an important role in the manufacture of ceramic parts (Zhang et al., 2022). Effective layer deposition requires appropriate slurry preparation, which has a significant impact on the surface morphology and the entire manufacturing process of ceramic products (Yamakov et al., 2002). Figure 3 shows the specimen's 3D model and layers manufacturing process.

Experimental setup

The LPBF system is shown in Figure 4. The system is equipped with an IPG YLR-500 fiber laser, which creates a laser beam with a

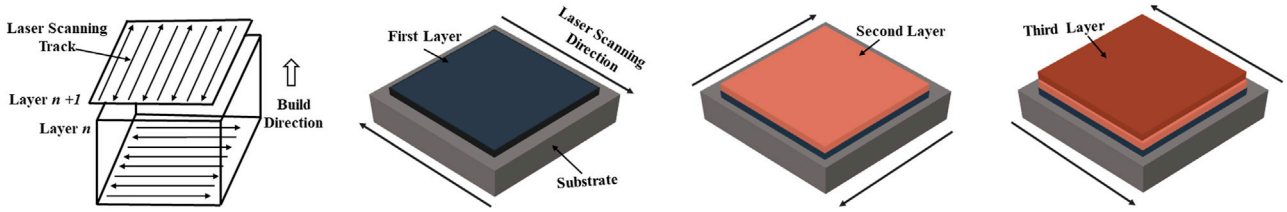


FIGURE 3
Laser scanning strategy and manufacturing method of the specimen.

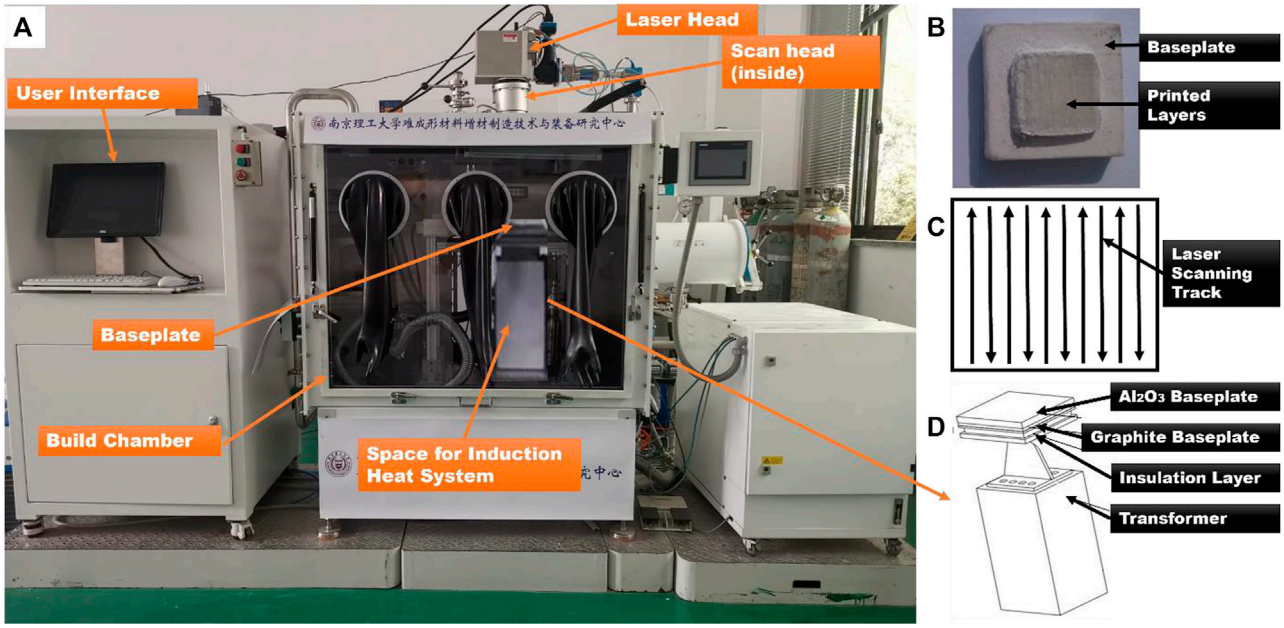


FIGURE 4
Experimental setup **(B)** Printed layers of ceramic specimen **(C)** Laser scanning strategy **(D)** Schematic of induction heating system.

wavelength of 1.06 μm and can reach a maximum power of 500 W in continuous mode. The laser is led through a scanner (SCANLAB intelliSCAN 20). The spot size of the focused laser beam is about 60 μm. The system is also integrated with the induction heating system (20 KW) produced by the Shanghai Bamac capable of rapid heating, and the maximum preheating temperature is about 1,000 °C.

The tests were designed based on varying laser power (p = 50 W–100 W). The remaining parameters, such as laser scanning speed (200 mm/s), layer thickness (50 μm), laser hatch spacing (50 μm), and scanning strategy (zigzag), remained unchanged. Table 1 provides the experimental process parameters. The size of every part was kept under 25 layers.

Measurements

Bruker D8 X-ray diffraction (XRD) was used to identify the structure, configuration, and quality of the samples. The XRD patterns were obtained at room temperature using Cu Kα radiation (λ = 1.5418Å) in continuous mode between 2θ = 10°–100°. The XRD was operated at tube current 40 mA and target voltage 40 kV at a scan speed of 2° min^{-1}. Scanning Electron Microscopy (SEM) was used to analyze the surface morphology and microstructure of fabricated parts. SEM and EDS analysis (Oxford Instrument), the specimens were gold-coated (by the Leica ACE coater for 5 min).

Results and discussions

Materials aspect

Scanning electron microscopy analysis of manufactured specimens using magnesia and alumina powders in various proportions revealed changes in density, porosity, and quality of the specimens produced. The effects of material change can be evaluated clearly as we increase the magnesia content, and the porosity increases at specific laser power (70 W). Increasing the

10.3389/fchem.2023.1034473

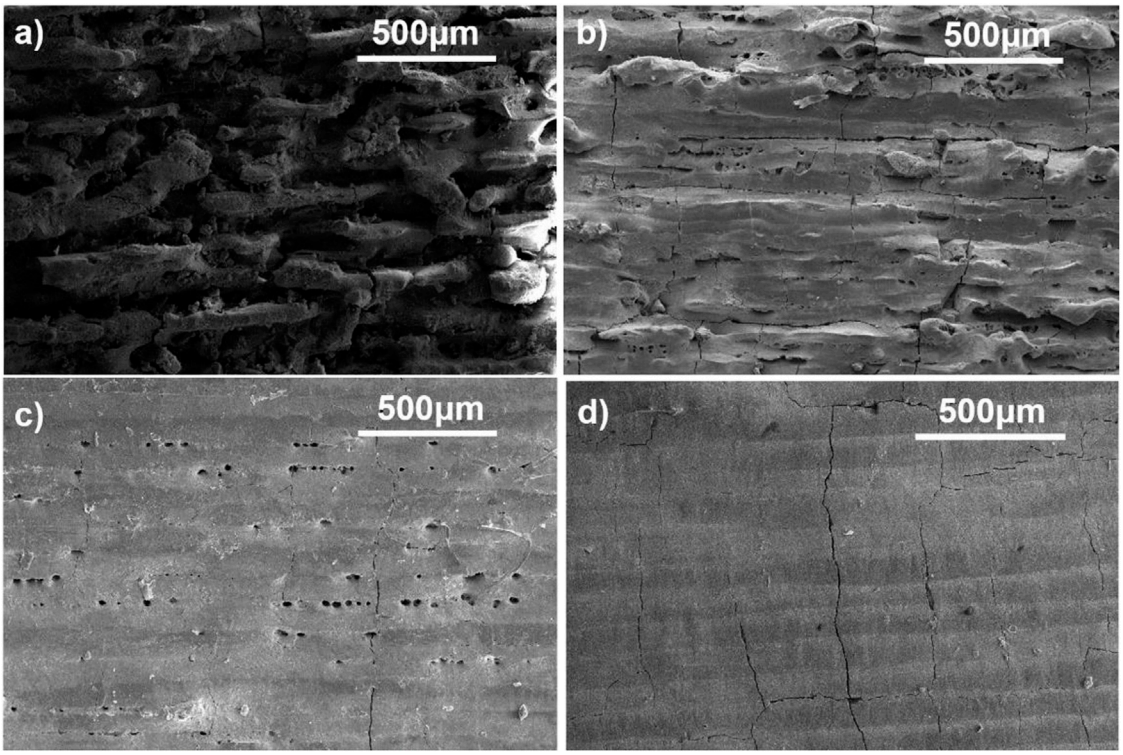


FIGURE 5
SEM **(A)** Alumina wt 20%: Magnesia wt 80% **(B)** Alumina wt 60%: Magnesia wt 40% **(C)** Alumina wt 75%: Magnesia wt 25% **(D)** Alumina wt 90%: Magnesia wt 10%, at laser power 70 W.

magnesia content in material proportion with the decrease in alumina wt%. Similarly, increasing the alumina content and decreasing the Magnesia content causes a significant change in the surface quality and layers of the printed article, as shown in Figure 5. The sample fabricated from powders with high magnesium content (80%) shows poor surface quality, with obvious surface defects such as cracks and partially molten powder, as shown in Figure 5A). By reducing the magnesia content to 40% and increasing the alumina content to 60%, the surface quality of the part improved slightly. However, a large number of pores and cracks can still be seen, as shown in Figure 5B). The pores observed on the surface of the specimens are small spherical pores with identical sizes. Most of these pores are located on the edges of melting tracks, which can be controlled by an effective overlap of the neighbouring tracks. To restrict the formation of pores on the melting tracks' edges, sufficient melting of the powder is required, as well as an efficient overlap of the adjacent tracks. The specimens made with a high alumina content show fewer surface defects and better melting conditions, which might be owing to alumina's lower melting point and better melting behaviour compared to magnesia. The number of pores is highly controlled by lowering the percent weight of magnesia and increasing the quantity of alumina to 10% and 90%, respectively, as shown in Figure 5D). The experimental results show that if we desire a porous-free surface of alumina-magnesia composite, we should choose the maximum wt% of alumina. However, there seems to be no improvement in crack prevention or control, indicating that changing the material composition alone is insufficient to eliminate surface defects.

Laser parameters aspect

The complete melting of powders is an important aspect of the LPBF process, which can eliminate several parts defects including cracks and porosity. To sufficiently melt the ceramic powders and improve the part's manufacturability by reducing partly melted flaws, a higher laser energy input is required. A higher laser power within a specific range produced more energy input which can control numerous surface defects such as poor melting, fractures, and porosity. We keep the material composition constant and change the laser power, to study the change in the morphology of alumina and magnesia composites. The effects of laser power can be evaluated in Figure 6, as we decrease the laser power the porosity increases, and the density decreases similarly as we increase the laser power the porosity reduces and density increases. Figure 6A, B show the poor melting of the powder with pores observed on the surface of the samples. When the powder particles partly melt but do not fuse or merge into the melting pool, voids between the particles occur, which can lead to insufficient melting defects including cracks and poor density. The distribution pores and formation of microcracks are greatly reduced when the laser power is increased to 90 W, as seen in Figure 6B, D. Obtaining higher energy density by increasing laser power enhances not only the melting state of the material but also the fluidity of the laser melting tracks, which greatly enhances the bonding strength of

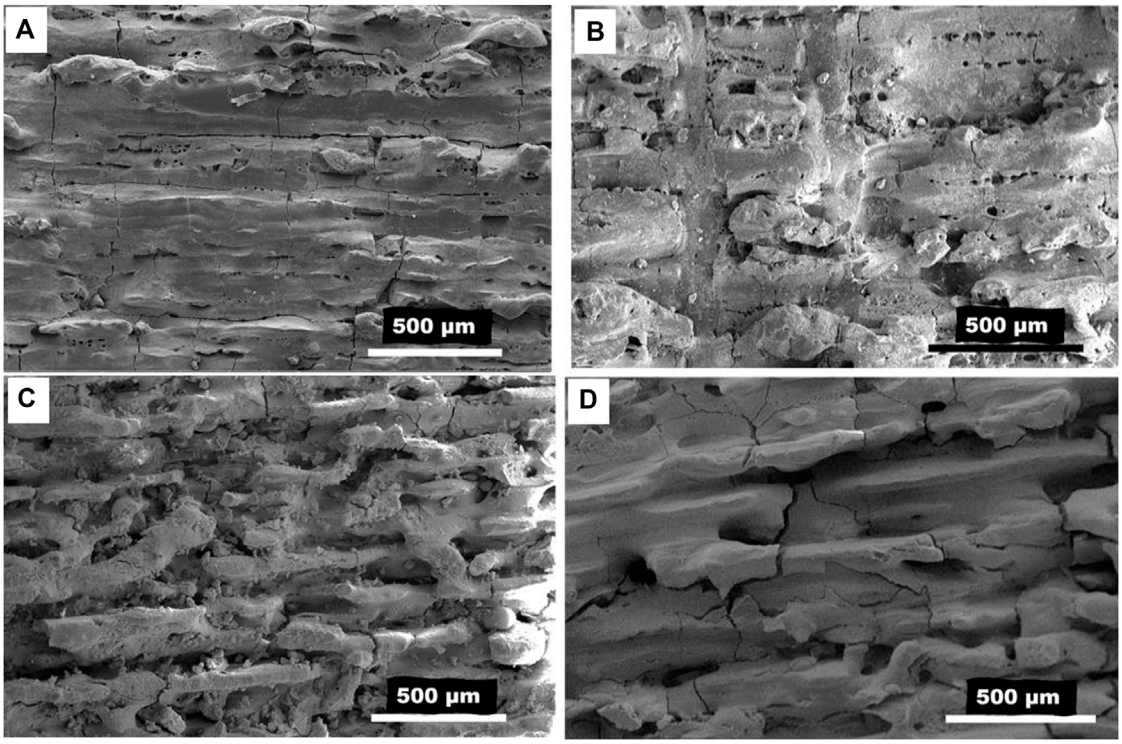


FIGURE 6
(A) Alumina wt% 60: Magnesia wt% 40 at Laser Power 70 W **(B)** Alumina wt% 60: Magnesia wt% 40, Laser Power 90 W **(C)** Alumina wt% 80: Magnesia wt% 20 at laser Power 70 W **(D)** Alumina wt% 80: Magnesia wt% 20 wt% at laser power 90 W.

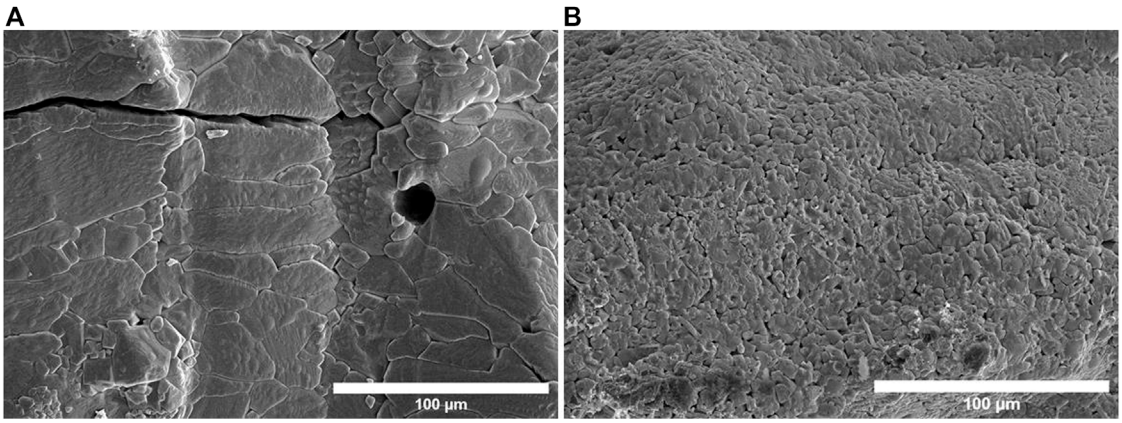


FIGURE 7
SEM Alumina-Magnesia Composite of 70 wt% Magnesia and 30 wt% alumina with Laser power **(A)** 50 W **(B)** 100 W.

the tracks. The stresses inside the layers are thus released more easily, which helps to reduce the driven force for crack growth (Zhang et al., 2022).

Laser power has also a significant influence on the grain structure formation on the surface of alumina and magnesia composite. In most cases, problems arise when the laser heat input is too low or too high. Heat input that is too high, either through excessive laser power or slow scan speed, can slow the cooling rate, resulting in excessive grain growth. Previous studies have shown that the crystalline grains produced during the laser melting process are rapid to develop, complex, and tightly compacted, which results in part defects such as fracture junctions and shrinkage (Chen et al., 2019) (Ullah et al., 2020). Large and irregular grains may possibly appear with low energy input, especially when printing ceramic parts, as a result of insufficient powder melting, quick cooling, or an unstable

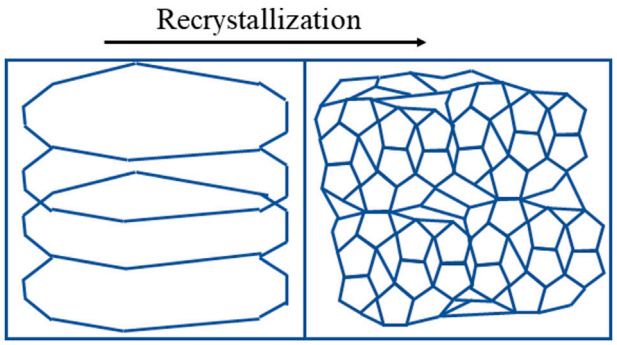


FIGURE 8
Schematic illustration of recrystallization by higher laser power.

microstructure (Ullah et al., 2022). Large grains can be observed in the sample produced with a lower laser power (50 W), which obviously subdivides and recrystallizes into small new grains by increasing the laser power to 100 W, as seen in Figure 7. The schematic illustration of grain recrystallization is shown in Figure 8. Grain growth is often undesirable in LPBF-manufactured components since it leads to several other defects. Previous research on the formation of grain structures shows that the grains produced by the laser melting process have several undesirable effects, including shrinkage and fractures (Chen et al., 2019). The size of cracks increases with the increase in grain size which may result in large fractures, as seen in Figure 7A). However, compared with coarse grains, small grains have some structural advantages as they increase the yield strength and macroscopic hardening of the material part (Yamakov et al., 2002).

Comparison of SiC and MgO loads effect

LPBF of alumina was also accomplished at various SiC loads up to 20 wt% which can be compared with the effect of MgO loads on alumina (Ur Rehman et al., 2022). The experimental results show that the influence of SiC on the microstructure and surface quality of alumina parts is relatively higher than the effect of MgO loads, as shown in Figure 9. When the SiC content was 10% or above, it initiated a chemical reaction between Al_2O_3 and SiC, causing structural and surface deformation, as seen in Figure 9A). This also resulted in excessive porosity and an undesirable appearance in the produced component. However, Figure 9C) shows that when the amount of SiC was less than 5%, the microstructure improved significantly during PBSLP with no effect of LPS or chemical interaction. By further decreasing the content of SiC to 0.5 weight percent, a crack pinning impact could be clearly seen, as shown in Figure 9D.

The increase of MgO content seemed to have a similar effect on the microstructure and surface morphology of alumina. However, the experimental findings suggest that SiC content has a greater and more evident impact than MgO loading because the effect of MgO content is seen when the MgO content is only increased to 10% or above, as shown in Figure 5. This might be due to magnesia's greater melting point and slower reaction rate than SiC with alumina. The impact of SiC loading, on the other hand, is only apparent when a very little

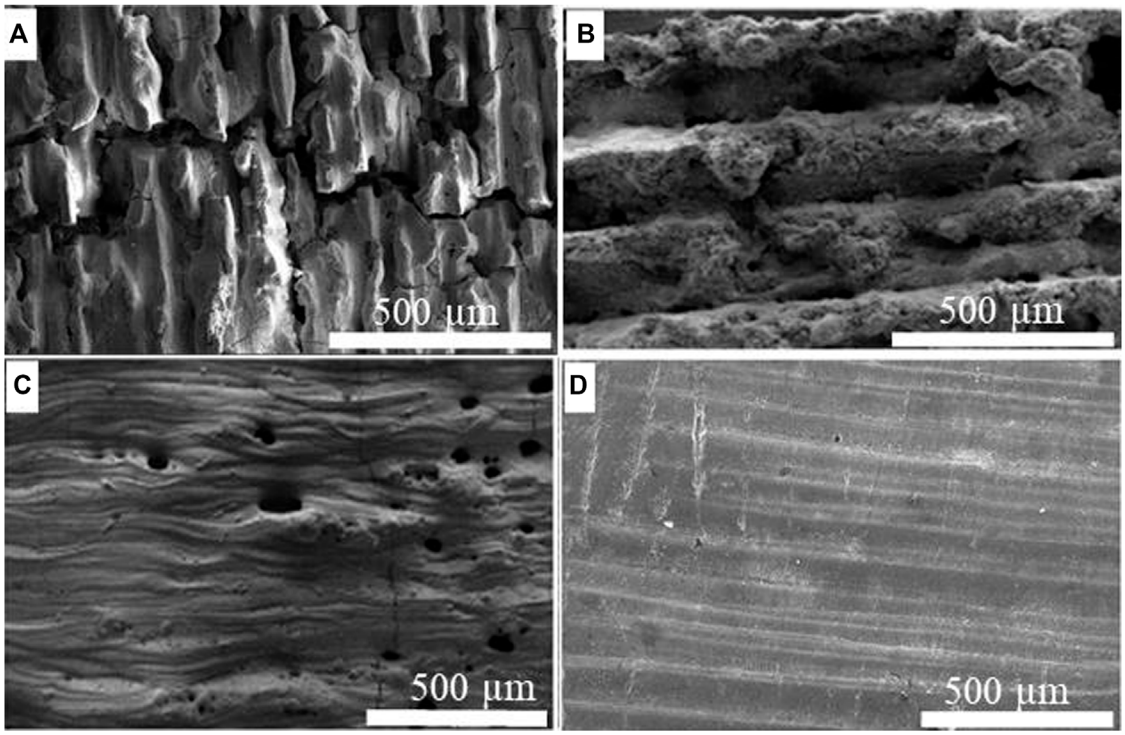


FIGURE 9
SEM of Al_2O_3/SiC samples at laser power 120 W **(A)** Al_2O_3 wt% 90, SiC wt% 10 **(B)** Al_2O_3 wt% 95, SiC wt% 5 **(C)** Al_2O_3 wt% 98, SiC wt% 2 **(D)** Al_2O_3 wt% 99.5, SiC wt% 0.5.

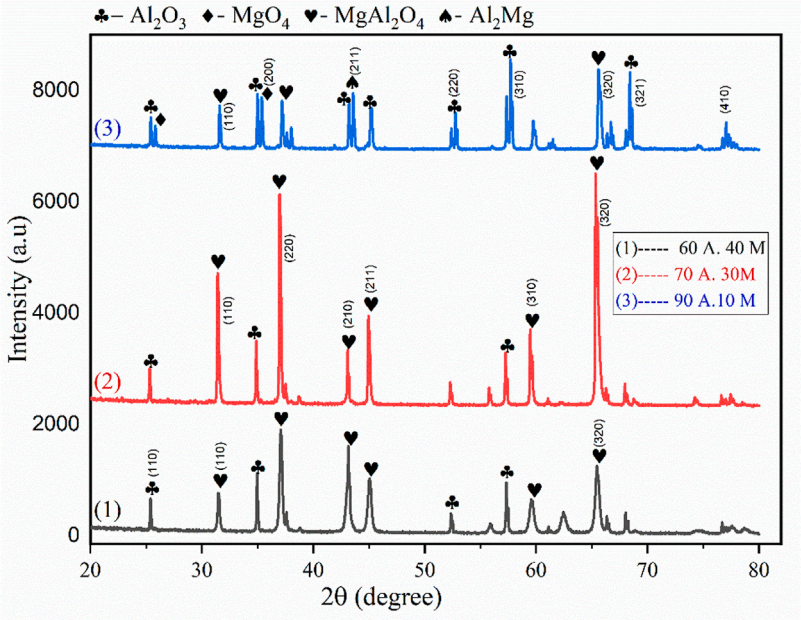


FIGURE 10
XRD of Al_2O_3-MgO specimens produced by LPBF process at laser power 100 W.

quantity of SiC (less than 2%) is added to the alumina powder. The chemical reaction of SiC with Al_2O_3 is increased by adding further SiC (up to 20%), resulting in surface deformation and porosity. The higher interaction of SiC to metal oxides may also lead to high weight loss, and porosity and can disturb the melt pool and the surface morphology of the printing parts. The following reactions are found to occur when Al_2O_3 interacts with SiC.

$$SiC_{(s)} + Al_2O_3\,(s) \rightarrow Al_2O_{(g)} + SiO_{(g)} + CO_{(g)} \quad (1)$$

$$2SiC\,(s) + Al_2O_3\,(s) \rightarrow Al_2O\,(s)\,(g) + 2Si_{(l)} + 2CO_{(g)} \quad (2)$$

$$3SiC_{(5)} + Al_2O_3\,(s) \rightarrow 2Al_{(l)} + 3Si_{(l)} + 3CO_{(g)} \quad (3)$$

XRD analysis

The XRD analysis shows that changing the material load has no obvious effect on the formation of $MgAl_2O_4$ composite, however, the density and overall microstructure of the composite are influenced. XRD peaks of the specimens formed with higher magnesia content (40wt%) show maximum peaks of $MgAl_2O_4$ with lower peak intensities of pure alumina, however, the sample produced of 30 wt % of magnesia shows higher peak intensities of $MgAl_2O_4$ with minimum peaks of MgO and pure alumina, as shown in Figure 10. In addition, the sample produced with higher Alumina content shows maximum peaks of Alumina with lower peak intensities of $MgAl_2O_4$ and MgO_4. These findings show that samples produced of 30 wt% of Magnesia and 70 wt% of Alumina have maximum solubility of the powder and a more refined structure of $MgAl_2O_4$ composite which agrees with the Eutectic Phase diagram of Alumina-Magnesia (Callister and Rethwisch, 2011). The following possible chemical reactions may occur during the interaction of Al_2O_3 and MgO at high laser power. During the interaction of Al_2O_3 and MgO at high laser power, the following chemical reactions may occur.

$$Al_2O_3\,(s) + MgO\,(s) \rightarrow MgAl_2O_4\,(s) \quad (4)$$

$$2MgO_{(s)} + 3Al_2O_3\,(s) \rightarrow 2MgO_4\,(s) + 3Al_2O_{(g)} \quad (5)$$

Conclusion

The LPBF of Al_2O_3 was accomplished at different MgO loads up to 80 wt%. The microstructure of the composites was significantly affected by the addition of Magnesia. Samples with 30 wt% of magnesia show reduced part defects with maximum content and higher intensity peaks of $MgAl_2O_4$ composite. However, the higher magnesia loads (≥40%) show maximum parts defects and low solubility. Laser power has a significant influence on the surface morphology of the composite samples. The Surface quality of the samples becomes better when the laser power is higher and magnesia loads are lower. The effect of SiC and MgO loads on the fabrication of Al_2O_3 parts was compared, and it was found that silicon carbide loads are more effective than magnesia loads. Surface defects were decreased by the addition of lower (less than 2%) silicon carbide powder.

Data availability statement

The original contributions presented in the study are included in the article/supplementary material, further inquiries can be directed to the corresponding authors.

Author contributions

AUR: Conceptualization, Methodology, Software, Validation, Formal analysis, Investigation, Resources, Data curation, Writing—original draft, Writing—review and editing, Visualization, Supervision, Project administration, Funding acquisition. AU: Conceptualization, Methodology, Software, Validation, Formal analysis, Investigation, Data curation, Visualization, Writing—original draft, Writing—review and editing. TL: Conceptualization, Methodology, Supervision, Project administration, Funding acquisition. RUR: Data curation, Visualization. MUS: Supervision, Project administration, Funding acquisition. All authors contributed to manuscript revision, read, and approved the submitted version.

Funding

This work was supported by the Frontier Leading Technology Basic Research Project of Jiangsu (No. BK20202007), the National Natural Science Foundation of China (Grant No.52005262), BK20190463 and No. B18028. This work was also supported by the National Natural Science Foundation of China (grant number 51775281). This project has also received financial support from the European Union's Horizon 2020 (H2020) research and innovation program under the Marie Skłodowska-Curie, grant agreement No. 101034425 and No. 764935.

Conflict of interest

Author AUR was employed by ERMAKSAN.

The remaining authors declare that the research was conducted in the absence of any commercial or financial relationships that could be construed as a potential conflict of interest.

Publisher's note

All claims expressed in this article are solely those of the authors and do not necessarily represent those of their affiliated organizations, or those of the publisher, the editors and the reviewers. Any product that may be evaluated in this article, or claim that may be made by its manufacturer, is not guaranteed or endorsed by the publisher.

References

Abdelmoula, M., Küçüktürk, G., Juste, E., and Petit, F. (2022). Powder bed selective laser processing of alumina: Scanning strategies investigation. *Appl. Sci.* 12 (2), 764. doi:10.3390/app12020764

Ahmed, A., Azam, A., Wang, Y., Zhang, Z., Li, N., Jia, C., et al. (2021). Additively manufactured nano-mechanical energy harvesting systems: Advancements, potential applications, challenges and future perspectives. *Nano Converg.* 8 (1), 37–42. doi:10.1186/s40580-021-00289-0

Aktrk, M., Boy, M., Gupta, M. K., Waqar, S., Krolczyk, G. M., and Korkmaz, M. E. (2021). Numerical and experimental investigations of built orientation dependent Johnson–Cook model for selective laser melting manufactured AlSi10Mg. *J. Mater. Res. Technol.* 15, 6244–6259. doi:10.1016/j.jmrt.2021.11.062

Ansari, P. a., Rehman, A. U., Pitir, F., Veziroglu, S., Mishra, Y. K., Aktas, O. C., et al. (2021). Selective laser melting of 316L austenitic stainless steel: Detailed process understanding using multiphysics simulation and experimentation. *Metals* 11 (7), 1076. doi:10.3390/met11071076

Baudin, C., Martínez, R., and Pena, P. (1995). High-temperature mechanical behavior of stoichiometric magnesium spinel. *J. Am. Ceram. Soc.* 78 (7), 1857–1862. doi:10.1111/j.1151-2916.1995.tb08900.x

Callister, W. D. (2000). *Fundamentals of materials science and engineering*. London: Wiley London.

Callister, W. D., and Rethwisch, D. G. (2011). *Materials science and engineering*. New York: John Wiley and Sons.

Chen, Z., Guraya, T., Darvish, K., Phan, M., and Pasang, T. (2019). Solidification during selective laser melting of Co-29Cr-6Mo alloy. *JOM* 71 (2), 691–696. doi:10.1007/s11837-018-3264-7

Deckers, J., Meyers, S., Kruth, J., and Vleugels, J. (2014). Direct selective laser sintering/melting of high density alumina powder layers at elevated temperatures. *Phys. Procedia* 56, 117–124. doi:10.1016/j.phpro.2014.08.154

Deckers, J., Vleugels, J., and Kruthl, J. (2014). Additive manufacturing of ceramics: A review. *J. Ceram. Sci. Technol.* 5 (4), 245–260. doi:10.4416/JCST2014-00032

Dezfoli, A. R. A., Lo, Y. L., and Raza, M. M. (2021). Microstructure and elements concentration of inconel 713lc during laser powder bed fusion through a modified cellular automaton model. *Crystals* 11 (9), 1065. doi:10.3390/cryst11091065

Dezfoli, A. R. A., Lo, Y. L., and Raza, M. M. (2021). Prediction of epitaxial grain growth in single-track laser melting of in718 using integrated finite element and cellular automaton approach. *Materials* 14 (18), 5202. doi:10.3390/ma14185202

Ganesh, I. (2013). A review on magnesium aluminate (MgAl2O4) spinel: Synthesis, processing and applications. *Int. Mater. Rev.* 58 (2), 63–112. doi:10.1179/1743280412y.0000000001

Gokcekaya, O., Ishimoto, T., Todo, T., Wang, P., and Nakano, T. (2021). Influence of powder characteristics on densification via crystallographic texture formation: Pure tungsten prepared by laser powder bed fusion. *Addit. Manuf. Lett.* 1, 100016. doi:10.1016/j.addlet.2021.100016

Harun, Z., Ismail, N. F., and Badarulzaman, N. A. (2012). Effect of MgO additive on microstructure of Al2O3. *Adv. Mater. Res.* 488, 335–339.

Khan, H. M., Waqar, S., and Ko, E. (2022). Evolution of temperature and residual stress behavior in selective laser melting of 316L stainless steel across a cooling channel. *Rapid Prototyp. J.* 28 (7), 1272–1283. doi:10.1108/rpj-09-2021-0237

Kingery, W. D. (1958). *Ceramic fabrication processes*. Berlin, Germany: Springer, 235.

Korkmaz, M. E., Gupta, M. K., Waqar, S., Kuntoglu, M., Krolczyk, G. M., Maruda, R. W., et al. (2022). A short review on thermal treatments of Titanium and Nickel based alloys processed by selective laser melting. *J. Mater. Res. Technol.* 16, 1090–1101. doi:10.1016/j.jmrt.2021.12.061

Korkmaz, M. E., Waqar, S., Garcia-Collado, A., Gupta, M. K., and Krolczyk, G. M. (2022). A technical overview of metallic parts in hybrid additive manufacturing industry. *J. Mater. Res. Technol.* 18, 384–395. doi:10.1016/j.jmrt.2022.02.085

Kruth, J. P., Mercelis, P., Van Vaerenbergh, J., Froyen, L., and Rombouts, M. J. R. p. j. (2005). Binding mechanisms in selective laser sintering and selective laser melting. *Rapid Prototyp. J.* 11, 1355–2546.

Kumar, M., and Sharma, V. (2021). Additive manufacturing techniques for the fabrication of tissue engineering scaffolds: A review. *Rapid Prototyp. J.* 27, 1230–1272. doi:10.1108/rpj-01-2021-0011

Liu, Z., Ketai, H., and Qingqiang, H. (2020). "The effect of hatch angles on the microstructure and mechanical properties of selective laser melting 316L stainless steel," in Proceedings of the 15th IEEE Conference on Industrial Electronics and Applications, Kristiansand, Norway, 09-13 November 2020 (IEEE), 165–169.

Mahmood, M. A. a., Ur Rehman, A., Lungu, M., Pitir, F., Salamci, M. U., Ristoscu, C., et al. (2022). Laser additive manufacturing of Co-Cr alloy and the induced defects thereof. *Int. J. Adv. Manuf. Technol.* 121 (1-2), 1385–1400. doi:10.1007/s00170-022-09395-7

Peng, W., Chen, Z., Yan, W., Schaffoner, S., Li, Y., et al. (2021). Advanced lightweight periclase-magnesium aluminate spinel refractories with high mechanical properties and high corrosion resistance. *Constr. Build. Mater.* 291, 123388. doi:10.1016/j.conbuildmat.2021.123388

Prakash, C., Singh, S., Kopperi, H., Ramakrihna, S., and Mohan, S. V. (2021). Comparative job production based life cycle assessment of conventional and additive manufacturing assisted investment casting of aluminium: A case study. *J. Clean. Prod.* 289, 125164. doi:10.1016/j.jclepro.2020.125164

Rahaman, M. N. (2017). *Ceramic processing and sintering*. Boca Raton, Florida, United States: CRC Press.

Redwood, B. (2018). *Additive manufacturing technologies: An overview*. Berlin, Germany: Springer, 201.

Rehman, A. U., Mahmood, M. A., Pitir, F., Salamci, M. U., Popescu, A. C., and Mihailescu, I. N. a. (2021). Mesoscopic computational fluid dynamics modelling for the laser-melting deposition of aisi 304 stainless steel single tracks with experimental correlation: A novel study. *Metals* 11 (10), 1569. doi:10.3390/met11101569

Rice, R. W. (2017). *Ceramic fabrication technology*. Boca Raton, Florida, United States: CRC Press. doi:10.1201/9780203911020

Sarkar, R. (2010). Refractory applications of magnesium aluminate spinel. *Interceram Refract. Man.* 1, 11–14.

Sathiyakumar, M., and Gnanam, F. (2003). Influence of additives on density, microstructure and mechanical properties of alumina. *J. Mater. Process. Technol.* 133 (3), 282–286. doi:10.1016/s0924-0136(02)00956-1

Schwentenwein, M., and Homa, J. (2015). Additive manufacturing of dense alumina ceramics. *Int. J. Appl. Ceram. Technol.* 12 (1), 1–7. doi:10.1111/ijac.12319

Sing, S. L., Yeong, W. Y., Wiria, F. E., Tay, B. Y., Zhao, Z., Zhao, L., et al. (2017). Direct selective laser sintering and melting of ceramics: A review. *Rapid Prototyp. J.* 23 (3), 611–623. doi:10.1108/rpj-11-2015-0178

Stewart, R., and Bradt, R. (1980). Fracture of single crystal MgAl 2 O 4. *J. Mater. Sci.* 15 (1), 67–72. doi:10.1007/bf00552428

Sun, Q. D., Sun, J., Guo, K., Waqar, S., Liu, J. W., and Wang, L. S. (2022). Influences of processing parameters and heat treatment on microstructure and mechanical behavior of Ti-6Al-4V fabricated using selective laser melting. *Adv. Manuf.* 10, 520–540. doi:10.1007/s40436-022-00389-y

Ullah, A., Ur Rehman, A., Salamci, M. U., Pıtır, F., and Liu, T. (2022). The influence of laser power and scanning speed on the microstructure and surface morphology of Cu2O parts in SLM. *Rapid Prototyp. J.* 28 (9), 1796–1807. doi:10.1108/rpj-12-2021-0342

Ullah, A., Wu, H., Rehman, A. U., Zhu, Y., Liu, T., and Zhang, K. (2020). Influence of laser parameters and Ti content on the surface morphology of L-PBF fabricated Titania. *Rapid Prototyp. J.* 27 (1), 71–80. doi:10.1108/rpj-03-2020-0050

Ur Rehman, A., Saleem, M. A., Liu, T., Zhang, K., Pitir, F., and Salamci, M. U. (2022). Influence of silicon carbide on direct powder bed selective laser process (Sintering/Melting) of alumina. *Materials* 15 (2), 637. doi:10.3390/ma15020637

Wang, Y., Mushtaq, R. T., Ahmed, A., Ahmed, A., Rehman, M., Rehman, M., et al. (2022). Additive manufacturing is sustainable technology: Citespace based bibliometric investigations of fused deposition modeling approach. *Rapid Prototyp. J.* 28 (4), 654–675. doi:10.1108/rpj-05-2021-0112

Wang, Y., Zhang, Q., Zhu, Z., Lin, F., Deng, J., Ku, G., et al. (2017). Laser streaming: Turning a laser beam into a flow of liquid. *Sci. Adv.* 3 (9), e1700555. doi:10.1126/sciadv.1700555

Waqar, S., Guo, K., and Sun, J. (2022). Evolution of residual stress behavior in selective laser melting (SLM) of 316L stainless steel through preheating and *in-situ* re-scanning techniques. *Opt. Laser Technol.* 149, 107806. doi:10.1016/j.optlastec.2021.107806

Waqar, S., Guo, K., and Sun, J. (2021). FEM analysis of thermal and residual stress profile in selective laser melting of 316L stainless steel. *J. Manuf. Process.* 66, 81–100. doi:10.1016/j.jmapro.2021.03.040

Waqar, S., Sun, Q., Liu, J., Guo, K., and Sun, J. (2021). Numerical investigation of thermal behavior and melt pool morphology in multi-track multi-layer selective laser melting of the 316L steel. *Int. J. Adv. Manuf. Technol.* 112 (3-4), 879–895. doi:10.1007/s00170-020-06360-0

Wilkes, J., Hagedorn, Y. C., Meiners, W., and Wissenbach, K. (2013). Additive manufacturing of ZrO2-Al2O3 ceramic components by selective laser melting. *Rapid Prototyp. J.* 19, 1355–2546.

WIPO (2018). *4D printing: Printing ceramics from metals with selective oxidation*. Berlin, Germany: Springer.

Wu, H., Roberts, S. G., and Derby, B. (2001). Residual stress and subsurface damage in machined alumina and alumina/silicon carbide nanocomposite ceramics. *Acta Mater.* 49 (3), 507–517. doi:10.1016/s1359-6454(00)00333-5

Yamakov, V., Wolf, D., Phillpot, S. R., and Gleiter, H. (2002). *Dislocation processes and deformation twinning in nanocrystalline Al*. United States: Argonne National Lab.

Zhang, K., Liu, T., Liao, W., Zhang, C., Yan, Y., and Du, D. (2018). Influence of laser parameters on the surface morphology of slurry-based Al2O3 parts produced through selective laser melting. *Rapid Prototyp. J.* 24 (2), 333–341. doi:10.1108/rpj-12-2016-0201

Zhang, X., Zhang, K., Zhang, B., Li, Y., and He, R. (2022). Quasi-static and dynamic mechanical properties of additively manufactured Al2O3 ceramic lattice structures: Effects of structural configuration. *Virtual Phys. Prototyp.* 17 (3), 528–542. doi:10.1080/17452759.2022.2048340

Zheng, Y., Zhang, K., Liu, T., Liao, W., Zhang, C., and Shao, H. J. C. I. (2019). Cracks of alumina ceramics by selective laser melting. *Ceram. Int.* 45 (1), 175–184. doi:10.1016/j.ceramint.2018.09.149